communications earth & environment

Article

A Nature Portfolio journal

https://doi.org/10.1038/s43247-026-03189-5

Permafrost and wildfire carbon emissions indicate need for additional action to keep Paris Agreement temperature goals within reach

Christina Schädel[1] ✉, Thomas Gasser[2], Brendan M. Rogers[1], Rachael Treharne[1], Merritt R. Turetsky[3], Trevor Smith[1], Erin MacDonald[1] & Susan M. Natali[1]

Rapid Arctic warming is thawing carbon-rich permafrost, releasing greenhouse gases that accelerate climate change. Despite the importance of this feedback, permafrost-enabled global-scale models simulate only gradual, top-down thickening of the seasonally-thawed soil. This ignores abrupt permafrost thaw and intensifying fire regimes that combust soil carbon and further accelerate thaw. Here, we expand a compact Earth system model (OSCAR v3.0) enabling initial estimates of the impacts of abrupt thaw and wildfire, together with gradual thaw, on remaining carbon budgets consistent with the temperature goals of the Paris Agreement. Our model suggests that including permafrost thaw and fire-related carbon emissions reduces the remaining allowable carbon budgets from 2025 onward by 25 % ± 12 % for avoiding 1.5 °C and 17 % ± 7 % for avoiding 2.0 °C, relative to simulations without these processes. Accounting for these additional emissions is critical for setting emissions reduction targets aligned with the Paris Agreement.

Northern permafrost-affected soils are estimated to contain around 1460–1600 Pg carbon (C), of which 1035 ± 150 Pg C is found in the near-surface (uppermost 3 m) portion of those soils[1,2]. Rapid Arctic warming is already affecting this critical carbon store, warming permafrost by up to 1 °C per decade[3]. This warming makes permafrost more vulnerable to thaw and the carbon it contains vulnerable to decomposition and release into the atmosphere in the form of greenhouse gasses, particularly carbon dioxide (CO_2) and methane (CH_4).

Modeling studies consistently predict that permafrost thaw will result in substantial emissions this century. Ranging from less than 20 Pg C to more than 200 Pg C[4–9], published estimates reflect considerable ongoing scientific uncertainty as to the magnitude, timing and form (i.e. CO_2 versus CH_4) of permafrost carbon emissions. Nonetheless, they all indicate an emissions source of sufficient magnitude to have tangible implications for global climate and thus for near-term policy decisions[10]. Refining those estimates is therefore a clear research priority that requires not only improved availability of data (e.g., regarding ground ice content and the effects of CO_2 fertilization on primary productivity), but also incorporating existing knowledge and data into modeling efforts[11,12].

Drivers of permafrost carbon emissions

Existing estimates of permafrost carbon release focus almost exclusively on top-down thawing of permafrost, resulting in a thickening of the active layer (the seasonally thawed soil layer above the permafrost surface). This 'gradual thaw' is the most widespread mechanism of permafrost degradation and is expected to result in the loss of 24–69% of near-surface permafrost by 2100[13–17].

However, other mechanisms are well-recognized as important drivers of permafrost thaw yet remain absent from the architecture of permafrost carbon-enabled Earth System and other global-scale models[11]. Notable among these are thermokarst (hereafter used interchangeably with 'abrupt thaw') processes, in which the thawing of permafrost that contains excess ground ice results in uneven subsidence or even collapse of the ground surface and subsequent erosion[18–20]. While many abrupt thaw features - such as retrogressive thaw slumps and active layer detachments in upland areas or thermokarst lakes in lowland areas - are relatively small within the scale of the permafrost region, they can affect a large volume of permafrost carbon over a shorter timescale when compared to gradual thaw and are therefore an important component of predicting future permafrost carbon emissions[21].

[1]Woodwell Climate Research Center, Falmouth, MA, USA. [2]International Institute for Applied Systems Analysis (IIASA), Laxenburg, Austria. [3]Renewable and Sustainable Energy Institute, Department of Ecology and Evolutionary Biology, University of Colorado Boulder, Boulder, CO, USA.
✉e-mail: cschaedel@woodwellclimate.org

Permafrost conditions are also intricately linked to wildfire. Increasingly extreme wildfire seasons have been observed across the northern permafrost region in recent years and decades, driven by more frequent lightning strikes, changing fuel conditions, extended fire seasons, and more severe fire weather[22–26]. While many boreal and tundra ecosystems have evolved with recurring wildfires, the more frequent, deeper-burning fires of recent years have accelerated permafrost thaw, both by driving a temporary increase in active layer depth[27], promoting the formation of unfrozen layers within the permafrost table, known as taliks[28,29], and initiating the development of thermokarst features. For example, one study found an almost three-fold increase in the rate of thermokarst bog development in western Canadian boreal peatlands following fire[30], and wildfire was associated with nine times as much thermokarst formation per area and year compared with unburned areas in northern Alaska[31].

In addition to its effects on permafrost, fire directly liberates carbon to the atmosphere during combustion. While emissions from combustion are typically represented in global scale models, they are restricted to combustion of above-ground biomass and litter. However, in the northern boreal and tundra regions, as much as 80–90% of emissions from combustion come from below-ground material[32,33], meaning global-scale models tend to underestimate fire emissions across the tundra and boreal biomes by roughly an order of magnitude[34].

The absence of abrupt thaw and fire effects in global-scale models means that pan-Arctic estimates of permafrost emissions are at best incomplete. While one attempt has been made to estimate pan-Arctic emissions from abrupt thaw[21], this does not explicitly address the effects of fire. Under-representation of abrupt thaw and fire in global-scale models has resulted in medium confidence in estimates of the remaining carbon budgets consistent with the temperature goals of the Paris Agreement[35]. This not only results in an inadequate understanding of mitigation urgency, but it also impedes efforts to accurately assess the efficacy of climate policy pledges.

Towards a more comprehensive estimate of permafrost carbon release

Here, we use a novel modeling framework to simulate a more complete spectrum of permafrost carbon emissions through the 21st century, accounting for gradual thaw, abrupt thaw and wildfire. We also estimate the impact of permafrost carbon emissions on remaining carbon budgets consistent with the temperature goals of the Paris Agreement. To achieve this, we build upon a reduced-complexity Earth system model (OSCAR v3.0) that was developed to emulate gradual permafrost thaw from four Land Surface Models (LSMs[4,36]. We extend OSCAR by adding new modules to simulate abrupt permafrost thaw (following Turetsky et al.[21]), emissions from below-ground combustion (above-ground combustion is already represented in OSCAR), and post-fire-induced permafrost thaw. These new modules build on published observational studies and combine process-based understanding, projected changes in disturbance frequency, and syntheses of existing observational and experimental data. Full details of the model implementation and parameterization are provided in the Online Methods.

The extended OSCAR model represents gradual, abrupt, and post-fire permafrost thaw in a stepwise manner. Simulations are run sequentially, starting with gradual thaw alone and progressively adding abrupt thaw and fire-related processes. Each simulation is driven by annual global temperature and emissions trajectories from the Shared Socioeconomic Pathways (SSPs) to estimate temperature-driven permafrost degradation and associated carbon release. This approach allows direct comparison of the additional contribution of each disturbance process and their combined effect on remaining global carbon budgets consistent with the Paris Agreement temperature goals.

Results

Emissions from permafrost thaw

Previous work using a variety of future warming scenarios and representations of permafrost processes has provided a considerable range of estimates of cumulative permafrost emissions this century from gradual thaw (22–550 Gt CO_2; across low to high emissions scenarios[37] and references therein. 1 Pg C = $\frac{44}{12}$ Gt CO_2). Emissions between 2025 and 2100 estimated here for gradual thaw alone range from 108 ± 94 Gt CO_2e under high mitigation (SSP1–2.6) to 235 ± 197 Gt CO_2e under low mitigation (SSP4–6.0), which are consistent with this range. These totals account for the GWP of the 2.3% of emissions of emitted carbon mass that are released as CH_4, using time-dependent GWP values integrated from the year of emissions through 2100. When combined with gradual thaw, emissions from abrupt thaw, below-ground combustion, and fire-mediated thaw (hereafter 'under-represented processes') ranged from 387 ± 167 GtCO_2e to 624 ± 278 GtCO_2e depending on the warming scenario (Fig. 1, Supplementary Note 6; Supplementary Fig. 6.2, Supplementary Table 3). This represents an increase in CO_2e emissions of between 166 and 258% compared to mean emissions from gradual thaw alone. On a shorter timescale (2025–2050), mean total emissions (i.e., under-represented processes combined with gradual thaw) were between 105 ± 49 Gt CO_2e and 116 ± 56 Gt CO_2e, an increase of between 185% and 202% compared to emissions from gradual thaw alone.

Under-represented processes were 72% of 2025–2100 total emissions on average under SSP1–2.6 (a low warming/high mitigation scenario) compared to 62% under SSP4–6.0 (a high warming, low mitigation scenario; the remaining 28–38% of total emissions are accounted for by gradual thaw). However, total emissions were on average 237 Gt CO_2e lower under SSP1–2.6 compared with SSP4–6.0 by 2100. Abrupt thaw and fire-related processes (i.e., below-ground combustion and fire-mediated thaw) had similar contributions to cumulative emissions, respectively accounting for 34% and 38% of total emissions under SSP1–2.6, and 30% and 33% of total emissions under SSP4–6.0. Abrupt thaw resulted in substantially more CH_4 emissions than other processes (Supplementary Fig. 6.3), with CH_4 emissions associated with abrupt thaw contributing 75–88% to the overall CO_2e emissions (Supplementary Fig. 6.4). This is expected given that abrupt thaw involves land subsidence or erosion following degradation of ice-rich permafrost and thus often increases anaerobic carbon mineralization pathways such as methanogenesis.

The IPCC Sixth Assessment Report estimated a mean permafrost carbon feedback (i.e., the amplification of warming due to carbon release from permafrost) of 22 Pg C for each 1 °C global temperature increase by 2100 based on a wide range of scenarios (range: 3–41 Pg C °C^{-1} [35]). Here, the mean feedback for gradual thaw was estimated at 28 Pg C °C^{-1} (25th–75th percentile: 10–36 Pg C °C^{-1}, based on the three SSP scenarios and four LSM calibrations used here) which is within the range of the IPCC estimate (Fig. 2). Including under-represented processes, the total permafrost thaw and wildfire emissions feedback accounted for 63 Pg C °C^{-1} (25–75th percentile: 35–73 Pg C °C^{-1}).

Reductions in emission budgets

Emissions budgets reported here are defined as the maximum cumulative CO_2 emissions below which the specified temperature threshold is avoided (i.e., not exceeded). In addition to these 'avoidance' budgets (Supplementary Table 4a), simplified 'exceedance' budgets are also reported in Supplementary Note 1, Supplementary Fig. 1.3, and Supplementary Table 4b.

All thaw and fire processes (including gradual thaw and under-represented processes) reduced emissions budgets by 124 ± 62 Gt CO_2 for a 1.5 °C temperature threshold, and by 258 ± 96 Gt CO_2 for 2.0 °C, (Fig. 3). These reductions represent 25% ± 12% of the 'no permafrost' avoidance budget (i.e., with no permafrost carbon dynamics represented in the model) for 1.5 °C, and 17% ± 7% of that for 2.0 °C.

Gradual and abrupt thaw had similar impacts on remaining budgets. Gradual thaw alone reduced budgets for 1.5 °C and 2.0 °C by 37 ± 30 Gt CO_2 and 83 ± 58 Gt CO_2 respectively, while the stepwise addition of abrupt thaw caused a further reduction of 35 ± 19Gt CO_2 and 72 ± 24 Gt CO_2. Fire-related processes had a slightly larger stepwise impact, reducing 1.5 °C and 2.0 °C budgets by a further 51 ± 23 Gt CO_2 and 103 ± 32 Gt CO_2 respectively. The magnitude of the reductions for both temperature goals was

influenced strongly by the LSM used to drive the gradual permafrost thaw emulator, with greater budget reductions associated with JSBACH (Supplementary Fig. 1.2).

Discussion

Implications for climate change mitigation

The impact of including abrupt thaw, high-latitude fire, and post-fire thaw on total estimated permafrost emissions is possibly very substantial, more than doubling total cumulative emissions from permafrost-affected soils this century. For context, by the end of this century these projected annual permafrost emissions (7–15 Gt CO_2e yr^{-1} across mitigation scenarios) could reach or exceed the current total annual emissions of a high-emitting nation such as the United States (~6.2 Gt CO_2e in 2023; United States Environmental Protection Agency, 2025); in the case that U.S. annual emissions remain unchanged through the end of the century.

The reductions in remaining avoidance budgets due to the inclusion of all permafrost thaw and fire-related processes (124 ± 62 Gt CO_2 and 258 ± 96 Gt CO_2 for 1.5 °C and 2 °C, respectively) are equivalent to 25 ± 12% and 17 ± 7% of the 'no permafrost' budget for these temperature goals. Under-represented processes alone reduced the budgets for 1.5 °C and 2.0 °C by an additional 87 ± 38 Gt CO_2 and 175 ± 47 Gt CO_2 compared to gradual thaw alone.

These permafrost emission budget reductions represent substantial shares of the remaining carbon budgets reported by the IPCC. The IPCC Sixth Assessment Report (AR6[35]) and the Global Carbon Budget 2024[38] express remaining budgets as the amount of CO_2 that can be emitted with a 50% likelihood of limiting warming below each temperature target. In contrast, this study reports ensemble-mean budgets derived from model simulations that emulate process-based Earth system models, representing remaining emissions until the model reaches each temperature threshold. In AR6, the remaining global budgets from 2020 are 500 Gt CO_2 for 1.5 °C and 1350 Gt CO_2 for 2 °C, each corresponding to a 50% chance of staying below the respective temperature target. The AR6 budgets include a static estimate of the permafrost carbon feedback associated with gradual thaw but exclude abrupt thaw and fire-related emissions. Considering these under-represented processes only, the AR6 budgets would be reduced by 17% for 1.5 °C and by 13% for 2 °C. Updated from AR6, the *Global Carbon Budget 2024*[38] lists remaining budgets of 305 Gt CO_2 for 1.5 °C and 1155 Gt CO_2 for 2 °C starting in 2025. The contribution from under-represented processes alone accounts for 29% and 15% reductions. Given the consensus around the small size of the remaining carbon budget - regardless of the specific estimate used - the scale of these reductions presents a real challenge to mitigation efforts. This is a stark reminder of the urgency of implementing measures that can deliver deep, near-term cuts in greenhouse gas emissions. It is already well-established that the carbon budgets for 2 °C, and in particular for 1.5 °C, are vanishingly small. The additional impact of permafrost thaw and high-latitude wildfire estimated here only adds to the challenge of keeping within these budgets. Nonetheless, the risks of allowing global average temperature increase to consistently exceed 1.5 °C, and the benefits of pursuing more ambitious mitigation, are becoming increasingly clear and challenging at the same time (IPCC, 2018). Nowhere is this better illustrated than in the northern permafrost region, where a 1.5 °C global average temperature increase translates to a regional temperature increase of more than 3 °C, and where natural and human systems are already facing extreme levels of disruption due to climate change.

The small size of the remaining carbon budget, and the encroachment upon it by permafrost thaw and wildfire, raises complex questions around equitable use of this remaining budget. While such questions are outside of the scope of this work, it is notable that permafrost emissions on the timescale relevant to the goals of the Paris Agreement are the result of cumulative anthropogenic emissions so far. Responsibility for permafrost emissions should arguably not therefore fall squarely on regions within which permafrost is found, but rather align with contribution to historical anthropogenic emissions.

Considering longer timescales, it is notable that even with considerable mitigation efforts the majority of total permafrost and fire-related emissions occur in the latter part of this century (more than 65% of 2025–2100 emissions occur after 2050 under SSP1–2.6), while the 1.5 °C threshold has already been exceeded for one year in 2024 (WMO 2024) and is expected to be reached consistently in the 2030s. Further, the long timescale of emissions from thawed permafrost dictates that the impact of permafrost thaw on global climate will continue to increase post-2100. It is therefore important that the longer-term implications of earth system feedbacks such as these, including for intergenerational justice, are considered alongside the urgent need for action on the 1.5 °C goal.

Importantly, even if higher global warming temperatures are avoided, permafrost carbon emissions will continue to be emitted long after, leaving future generations to manage the consequences. Future research is needed to better understand the long-term impacts of permafrost emissions after peak global temperatures are reached, which will help inform future mitigation strategies.

Key assumptions and caveats

In implementing the processes representing abrupt thaw (Methods 2), below ground combustion (Methods 3), and fire-induced thaw (Methods 4) in an additive, stepwise manner, we have made assumptions about the extent to which these processes can be separated in OSCAR. This is to an extent justified by the structure of OSCAR, which models only change due to perturbation. For example, in the case of the abrupt thaw module, the baseline emissions due to abrupt thaw as estimated in ref. 21 are not replicated in OSCAR because they would also happen in the absence of climate change. Instead, emissions from additional abrupt thaw above that baseline resulting from global temperature change alone are modeled. That this model structure does not result in substantial overestimation of net emissions from all processes is also indicated by the total area affected by either abrupt thaw or fire.

However, unlike the new processes integrated into OSCAR, gradual thaw cannot be expressed in terms of area, as the gradual thaw emulator operates on a pool of carbon totaling between 389 Pg C and 691 Pg C depending on the LSM configuration used (Methods[4]). The carbon pools defined within the gradual thaw emulator are smaller than current estimated values, even for near-surface (upper 3 m) permafrost, while at least a portion of the emissions resulting from features such as retrogressive thaw slumps, which the abrupt thaw modules aim to represent, are likely to originate from deeper carbon pools[2,21,39]. Nonetheless, the lack of any explicit means of separating the gradual thaw carbon pool from new thaw processes in the model remains a limitation of the approach taken here.

Data availability continues to present a barrier to future projections concerning the processes addressed here. Abrupt thaw refers to a complex set of processes often involving thermokarst (ground subsidence) and rapid ecological state change[21] and is inherently tied to ice-rich permafrost[40]. Understanding the spatial distribution and variation in ground ice has been a persistent challenge, but new remote sensing and mapping techniques[41,42] may allow for finer-scale data on ground ice to be incorporated into future modeling not only of abrupt thaw rates but also how they result in different surface expressions (i.e., thaw lakes versus wetlands) in different terrain conditions. For this study, we follow the approach taken by Turetsky et al.[21], which reduce the complexity of dozens of individual abrupt thaw processes into three generalized scenarios including thaw in lowland mineral terrain that often lead to thaw lakes, in lowland organic terrain that often result in thaw wetlands, and in hillslope terrain that often result in erosional features such as gullies or active layer detachments. Also inherent to this study is the assumption that changes in the rate of abrupt thaw will track the rates of gradual thaw in this (see also Supplementary Table 5). This approach is a reasonable first step given that the sensitivity of abrupt thaw to climate change is not well understood. While our consideration of abrupt thaw does include changes in carbon fluxes occurring with historical and contemporary patterns of ecosystem succession over time, we are not able to consider dynamic vegetation changes expected to occur in the permafrost

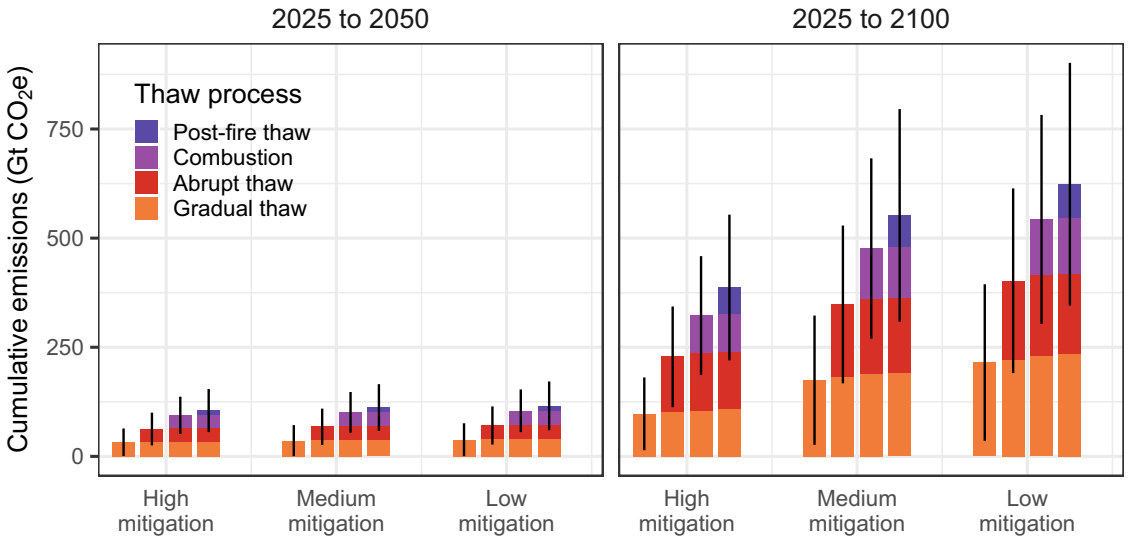

Fig. 1 | Cumulative permafrost carbon emissions under mitigation pathways. Cumulative permafrost carbon emissions (Gt CO_2e) from 2025 to 2050 and 2025 to 2100 across different SSPs (high mitigation = SSP1–2.6, medium mitigation = SSP2–4.5, low mitigation = SSP4–6.0). Bars show weighted multi-model ensemble means of the four LSMs. Stacked colors represent the stepwise addition of thaw processes in the simulations (individual bars within each mitigation group). Gradual thaw (orange), + abrupt thaw (red), + combustion (purple), and + post-fire (blue). The sequential stacking shows cumulative contribution of each process to total permafrost emissions per simulation. Error bars indicate weighted standard deviation of all emissions per simulation.

region with future warming and how it could alter known abrupt thaw succession. Similarly, despite wildfire being a comparatively well studied disturbance type across the boreal biome in particular, the limited availability of projections of future burned area ($n = 12$) necessitated a simplified approach, whereby we assume a linear increase in annual area burned in response to temperature change at a rate that is consistent across the different regions and ecosystems of the tundra and boreal biomes. Despite these challenges, we believe that this study provides useful first-order estimates that illustrate the possible magnitude of the emissions from permafrost thaw and wildfire processes that are rarely represented in global scale models.

Implications for future research

While existing understanding and observations have facilitated the first-order approach taken here, a number of barriers remain to fully incorporating abrupt thaw, fire and post-fire thaw into global-scale models[12]. The environmental context, other effects of a changing climate, such as altered precipitation regimes, and the mechanisms through which permafrost carbon is exposed to decomposition has an important influence on the timing and form (CO_2 or CH_4) of permafrost emissions[40,43,44]. Geomorphological and hydrological changes that result from permafrost thaw, such as subsidence, wetting or drying, combined with site-specific factors such as topography, can all influence the speed and product of in-situ decomposition, as well as the rate of carbon loss through lateral flow[45]. Similarly, the mechanisms through which changes in future climate, vegetation, and ignition patterns influence wildfire regimes is uncertain, as evidenced by the spread of results from our meta-analysis (Supplementary Fig. 3.1). While attempts to model these mechanisms require advanced process-based models (from which our work could also benefit), the first-order results reported here highlight their importance. In particular, the considerable impact of abrupt permafrost thaw on carbon budgets estimated here is in part attributable to the higher proportion of emissions released in the form of CH_4 as projected by Turetsky et al.[21] and implemented here (Supplementary Fig. 6.4). This emphasizes the critical need for a more precise understanding of the factors that determine the form of carbon release from permafrost thaw processes, and for a more detailed representation of those factors in global-scale models. Similarly, improved understanding of abrupt thaw drivers would facilitate a more coherent and robust treatment of the interaction between fire and abrupt thaw processes.

Conclusion

The results reported here highlight the tension between the necessity of achieving the temperature goals of the Paris Agreement and the declining feasibility of those goals in the absence of a step-change in global mitigation efforts. This in turn highlights a need for research addressing the implications of overshooting (temporarily exceeding) those temperature goals. In the case of permafrost thaw and high-latitude wildfires, emissions will continue on centennial timescales, even in the event of a subsequent decline in global average temperatures[46]. Furthermore, some local-scale consequences of thaw, such as ground subsidence, are irreversible - as is permafrost carbon loss, on human timescales. A more detailed and better-quantified understanding of how the magnitude, duration and timing of an overshoot affects the consequences of permafrost thaw and wildfire is needed.

Methods

OSCAR

OSCAR is an Earth system model of reduced complexity with core modules calibrated to emulate the behavior of more complex models[4,36,47]. The full description of OSCAR v2.2, including details on structure, equations and calibration, can be found in Gasser et al.[36]. We used OSCAR v3.0, which includes a permafrost carbon module that emulates gradual thaw as represented in four LSMs: JSBACH, ORCHIDEE-MICT, and two versions of JULES[48–51]. Permafrost carbon is defined within this emulator as carbon that was frozen and thus inactive during preindustrial times, with an initial pool size of between 389 Pg C and 691 Pg C. A full description of the gradual thaw emulator, including definitions and values for these and other parameters, are defined and reported in Gasser et al.[4]. The gradual thaw emulator was unchanged here.

OSCAR v3.0 was extended here through the inclusion of new modules addressing abrupt thaw (Method Section "Abrupt thaw module") and fire in the boreal and tundra biomes (Fig. 4). The fire module comprises a first-order estimate of emissions from combustion of below-ground carbon during fire (Method Section "Combustion emissions module" & Supplementary Note 3) and estimates of emissions from additional permafrost thaw driven by fire activity (Method Section "Post-fire permafrost thaw module" & Supplementary Notes 4, 5).

We used the global Shared Socioeconomic Pathways (SSP) data and scenarios to drive the model[52]. We included four scenarios (SSP1–2.6, SSP2–4.5, SSP4–6.0, SSP5–8.5) to span a wide range of futures, with

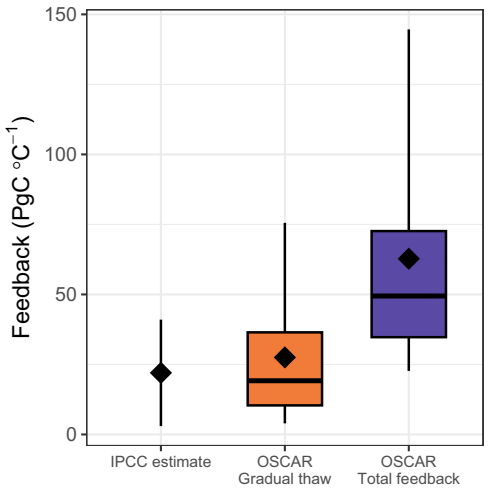

Fig. 2 | Permafrost carbon feedback per degree of warming. Permafrost carbon feedback per degree of increase in global average temperature (Pg C °C^{-1}) for gradual permafrost thaw (orange) and for total permafrost emissions (i.e., gradual + abrupt thaw + below-ground combustion + fire-induced thaw emissions; blue) this century. Feeback is calculated for CO_2 only relative to 2015 and includes SSP1–2.6, SSP2–4.5, and SSP4–6.0. The IPCC estimate (left) is the permafrost feedback mean value and range used in the Working Group I contribution to the Sixth Assessment Report of the IPCC.

SSP5–8.5 used only as a very high emissions, low-likelihood upper bound. Fossil CO_2 and CH_4 emissions were only used to drive the model; atmospheric concentrations of all other greenhouse gasses were prescribed in the model. Radiative forcings of near-term climate forcers (ozone and aerosols) and albedo effects (black carbon on snow and land-cover change) were also prescribed based on SSP data. To ensure that the emissions used to drive the model reproduced the atmospheric concentrations of CO_2 and CH_4 from the SSP scenarios in the absence of a permafrost feedback, we first ran a concentration-driven simulation with all permafrost feedback processes switched off. This provided the compatible fossil CO_2 and CH_4 emissions that were used in the subsequent emissions-driven runs to drive the model without permafrost and with permafrost processes switched on. Land-use and land-cover change data came from the LUH2 data set[53].

OSCAR is not spatially explicit. However, as described further below, in order to implement the abrupt thaw module, which builds upon the approach taken in Turetsky et al.[21], and to facilitate a similar first-order approach with regard to fire, we have used spatial data to constrain our calculations of carbon vulnerability or emissions within OSCAR. All simulations are performed at annual temporal resolution, and model outputs (e.g., temperature, fluxes, and emissions) are reported as annual values.

Emissions as CO_2 equivalent

The OSCAR model calculates the climate impact of emissions (including permafrost and fire-related emissions) internally, reflecting that impact in its temperature output with any use of CO_2e metrics. For the specific purpose of communicating the climate impact of the emissions output by OSCAR, however, we calculated CO_2e based on Global Warming Potential (GWP), defined as the ratio of the radiative forcing of a pulse emission of a gaseous species (in this case CH_4) to the radiative forcing of an equivalent emission mass of CO_2 across the same time period (Eq. (1)[54]). Methane emissions were multiplied by the GWP for the time period between the year of emission and 2100 to obtain the equivalent carbon dioxide emission (CO_2e, Supplementary Fig. 6.1). An exponential function was used to interpolate GWP between commonly used 20 and 100-year values[54,55] (Supplementary Fig. 1.4):

$$CO_{2e} = CH_4 * \left(\frac{130}{e^{(0.01384 * T_{GWP}) + 0.16}}\right) \quad (1)$$

Where T_{GWP} is equal to 2100 less the year of emission. For example, CH_4 emitted in 2050 was multiplied by its 50-year GWP to give CO_2e.

Abrupt thaw module

Overall structure. The abrupt thaw module builds upon the core assumptions and behavior of the models reported in Turetsky et al.[21]. These models represent the development of thermokarst features which can ultimately affect a relatively large area (i.e., >~100 m^2 per feature). In brief, this study used three numerical inventory models to represent abrupt thaw in hillslope, mineral lowland, and organic lowland landscapes. The total area of each landscape associated with abrupt thaw was defined through spatial analysis[40], while change detection and remote sensing data were used to specify starting areas of stable ice-rich permafrost (which includes 'undisturbed' land and land that has re-formed permafrost following the maturation of thaw features), active thaw, and stabilized thaw features (features that are no longer actively expanding). Synthesis of remote sensing, palaeoecological data and—in the case of the transition from stable permafrost to active thaw—field observations were used to define rates of transition between these different thaw states. The influence of climate change was represented by increasing the transition rate between undisturbed permafrost and active thaw in line with the average output of permafrost-enabled LSMs, in turn forced by the Community Climate System Model 4 ESM (CCSM4). Estimates of carbon fluxes associated with each thaw state and landscape type were derived from synthesis of published literature (reported in Turetsky et al.[21]).

Here, we use a modeling framework to estimate the total area of each thaw state (stable, active, stabilized, and mature) within each of the landscape types outlined above as a function of temperature. The temperature response used was derived from the output of the models reported in Turetsky et al.[21] and the corresponding temperature projections from CCSM4. Emissions were calculated based on the area of each thaw and landscape type using the carbon flux parameters reported in Turetsky et al.[21].

Forcing

We used temperature response functions (Supplementary Fig. 2.1) for the area (Eq. (2)) of each abrupt thaw state (i.e., active thaw, stabilized thaw, mature thaw, and stable landscape) within each landscape type (i.e., hillslope, mineral lowland, or organic lowland) using model outputs from Turetsky et al.[21], in which abrupt thaw rates were parameterized to track projections over time of gradual thaw rates in eight permafrost-enabled LSMs[5]. In order to integrate the Turetsky et al.[21] abrupt thaw model into OSCAR (in which time cannot be used as a driving variable), we derived temperature response functions using the model output combined with global temperature anomalies from the Community Climate System Model (CCSM4.0), which was used to force the permafrost-enabled models used in McGuire et al.[5]. This enabled us to mirror Turetsky et al.[21] closely within OSCAR (Supplementary Fig. 2.2).

As the time periods prior to and following 2000 were parameterized separately in Turetsky et al.[21], it was not always possible to derive a single temperature response function that satisfactorily emulated the behavior of the models reported by Turetsky et al. at low levels of global average temperature increase (<1 °C). In these cases the area of stable permafrost was over-predicted (i.e., estimated to exceed the maximum area parameterized in Turetsky et al.), and/or the area of active thaw was under-predicted (i.e., estimated to drop below 0) prior to 2000. We therefore constrained the output within a realistic range (i.e., greater than 0 and less than the maximum area of the specified landscape type). These constraints affected only the period prior to 2000. All temperature ($T\ in^{\circ} Celsius$) responses were modeled as third-order polynomials using a self-starting model in RStudio[56]. Area refers to area undergoing abrupt thaw, dT is delta temperature with respect to preindustrial temperature; a, b, and c are derived parameters.

$$Area = a * \left(1.5 * dT^b\right) - \left(dT^c * b\right) \quad (2)$$

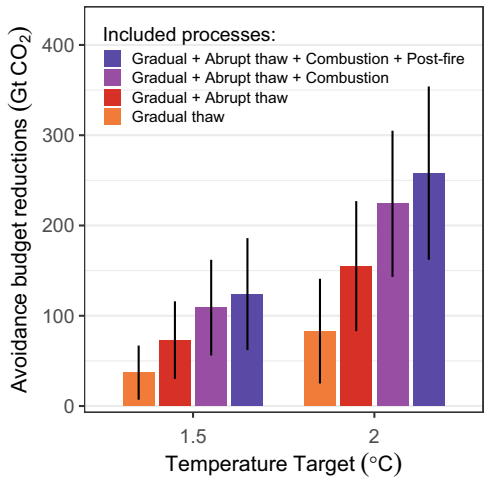

Fig. 3 | Reductions in remaining carbon budgets. Reductions (Gt CO_2) in remaining avoidance budgets for the 1.5 °C and 2 °C temperature targets, calculated relative to simulations with permafrost thaw and fire processes switched off (absolute values in Supplementary Table S4a). Bars show weighted multi-model mean results for simulations with different processes switched on, with error bars denoting the corresponding weighted standard deviations, both calculated across models, SSPs (excluding SSP5–8.5), and parameter configurations.

Emissions from abrupt thaw

In order to reproduce model assumptions and behavior, we used the parameters from Turetsky et al.[21] to calculate CO_2 and CH_4 emissions, including emissions from laterally transported dissolved organic carbon, from the area of each stage of abrupt thaw development in each landscape. These parameters were based on observational data obtained through literature review (full details in Turetsky et al. Supplementary Information).

Turetsky et al.[21] modeled both 'baseline' (no perturbation) emissions from abrupt thaw-prone landscapes and the change in those emissions due to perturbation (in this case from global average temperature increase). To align with the OSCAR framework, we therefore subtracted the net CO_2/CH_4 balance at a perturbation of 0 (defined in OSCAR as the absence of any increase in global average temperatures) from the emissions associated with abrupt thaw in OSCAR. This ensured we are modeling only the emissions associated with global warming perturbation.

Combustion emissions module

Overall structure. Because OSCAR already includes emissions from above-ground combustion, the combustion emissions module and results reported here are restricted to those originating from the combustion of below-ground material during fire (i.e., soil organic matter and belowground plant biomass). These combustion emissions are driven by burned area estimated as a proportion of total area of the tundra and boreal biomes[57]. Burned area is a primary factor in estimating emissions from high latitude fires[34,58].

Forcing. A temperature response function for total burned area change (Eq. (3)) was based on 38 estimates of burn metric change from 12 publications identified through a systematic literature search following methodology used by Phillips et al.[59] (Supplementary Note 3.1, Supplementary Fig. 3.1).

For each combination of region and Global Climate Model (GCM) reported in each publication, we retrieved temperature (T) data and a baseline burn metric (B_{base}; i.e., burned area, carbon emissions, or fire frequency) for a period of ~2000–2020, and the projected burn metric (B_{proj}) and temperature data through ~2075–2100. We included variation in years because both the climate system and fire regimes exhibit year-to-year variability and multi-decadal timeframes are required to ensure a robust average. For each combination of region and GCM the change in burn metric (B_Δ) was calculated per degree Celsius (°C^{-1}):

$$B_\Delta = \frac{(B_{proj} - B_{base})}{dT} \quad (3)$$

A final weighted average by burned area was used to drive a linear temperature response of burned area in the OSCAR model. The relationship between change in burn metric and change in burned area was assumed to be 1:1.

Emissions from combustion. Gross fire emissions were based on over 500 observations of below-ground carbon combustion, averaging 2.80 kg C m^{-2} for boreal sites and 1.81 kg C m^{-2} for tundra (Veraverbeke et al.[32] and references therein).

We did not directly modify net primary productivity (NPP; a core OSCAR process) in response to high latitude fire, but compensated for increased post-fire NPP by increasing CO_2 uptake relative to emission losses during a set post-fire recovery interval, parameterized based on crown fires in boreal North America (Supplementary Note 3.2).

Fire carbon emissions were partitioned into CO_2 and CH_4 using an emissions factor derived from Akagi et al.[60] following the approach used by Phillips et al.[59]. Because Akagi et al.[60] present emission factors relative to the combustion of dry matter (g kg^{-1}) rather than as a proportion of total emissions, we used these emissions factors to calculate the relative proportions of emissions which were CO_2 and CH_4, adjusted by molecular weight. This resulted in carbon-specific emissions factors of 0.84 for CO_2 and 0.0093 for CH_4 (i.e., a ratio of 90:1).

Post-fire permafrost thaw module

Post-fire permafrost thaw is addressed through three distinct pathways. Firstly, burned area is used to estimate an additional area of active abrupt thaw (i.e., in addition to that estimated within the abrupt thaw module), as well as the subsequent changes in the areas of stabilized and mature thaw features (as additional abrupt thaw transitions to these stages; Method Section "Fire-induced abrupt thaw"). Emissions from the annual additional area of active, stabilized and mature abrupt thaw features were calculated using parameters derived from Turetsky et al.[21]. A second 'progressive thaw' pathway describes the total loss of near-surface permafrost (upper 3 m of the permafrost table) on a decadal timescale following fire (Method Section "Fire-induced progressive thaw"). Finally, the predominant pathway is 'transient thaw'. This describes a gradual increase in thaw depth, peaking within a decade of fire, following which thaw depth recovers to pre-fire levels on a decadal timescale (Method Section "Fire-induced transient thaw"). Emissions from progressive and transient post-fire thaw were calculated following the approach of the gradual thaw permafrost emulator[4] (Supplementary Note S5).

Fire-induced abrupt thaw

Overall structure. Because data describing fire impacts on thermokarst formation are limited, we used post-fire changes in ground temperatures, combined with air temperature anomaly, to estimate fire-induced change in abrupt thaw area, as described further below, with further detail in Supplementary Note 4. Total burned area (Method Section "Combustion emissions module") was used to estimate annual burned area in the same spatial subdivisions used within the abrupt thaw module (i.e., thermokarst-prone regions of mineral lowlands, organic lowlands, and hillslopes; Supplementary Fig. 4.2). A fraction of annual burned area in those landscapes was subsequently designated as active abrupt thaw, using an estimate of the average increase in ground temperature following fire. Given expected increases in fire severity due to climate warming, we increased ground heating due to fire with warming (Supplementary Fig. 4.3). In the absence of data correlating post-fire ground temperature change with abrupt thaw initiation or expansion rates, we

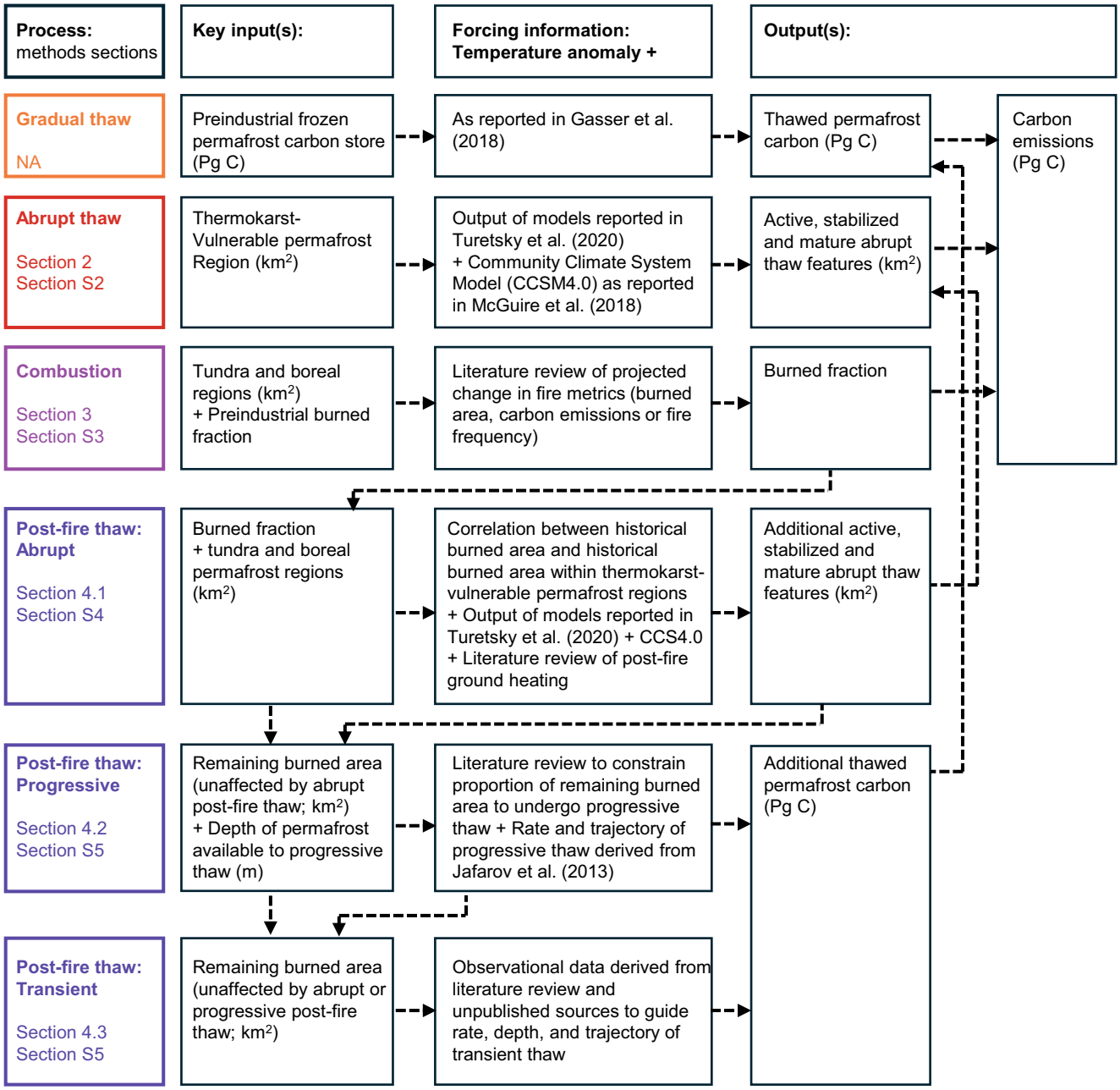

Fig. 4 | Conceptual framework for permafrost and fire processes in OSCAR. Conceptual figure illustrating the different processes through which OSCAR is extended here, with gradual thaw (already represented in OSCAR through the permafrost carbon emulator reported in Gasser et al.[4]) included for context. This figure demonstrates the linkages and interactions between different processes but does not provide a complete picture of how each process operates. 'Key inputs' describe the primary quantities on which the process acts. 'Forcing information' describes the information underlying the mechanism through which the process acts on the specified key inputs, in addition to global average temperature anomaly. 'Outputs' describe the quantities from which carbon emissions are calculated. Note that 'combustion' represents only below-ground combustion, as above-ground combustion was already integrated into OSCAR v3.0. Colors in the left column correspond to the processes shown in Figs. 1–3.

used the response of active abrupt thaw area in different landscape types to global average air temperature anomaly (derived from Turetsky et al.[21] as a proxy for the response to modeled post-fire ground heating (Supplementary Fig. 4.4). While annual thermokarst-prone burned area was calculated separately for different landscape types, the fraction of that area designated as active abrupt thaw was consistent across landscape types.

Active abrupt thaw area following fire was subsequently allowed to transition to stabilized thaw features before re-aggregating permafrost, following the parameterization of these transitions outlined in Turetsky et al.[21].

Response derivation. Annual burned area in thermokarst-prone landscapes was estimated using a linear correlation with total burned area across the boreal and tundra biomes (Supplementary Fig. 4.2). This correlation was derived from observational data describing annual burned area across two decades (1997–2016[61]), overlaid with spatial data describing vulnerability to thermokarst and landscape type (hillslope, mineral lowland or organic lowland[40].

The linear response of active abrupt thaw area to global average temperature anomaly (used as a proxy for the response of fire-induced abrupt thaw to modeled post-fire ground heating) was derived from the model output of Turetsky et al.[21] combined with global temperature anomaly from

CCSM4.0 (Supplementary Fig. 4.3). This approach is similar to that described in Method Section "Forcing", but simplified through the assumption of a linear response, and equates to an increase in the total area of active abrupt thaw features of between 1.17% $°C^{-1}$ (hillslopes) to 3.32% $°C^{-1}$ (mineral lowlands).

The range of values for post-fire change in ground temperature was informed by observational data describing changes in ground temperature within 1 m of the ground surface following fire (minimum and mean values; Supplementary Table 1). Average minimum and mean values of 2 °C and 3.3 °C, respectively, were weighted by biome and by measurement depth (weighted linearly by distance from a 50 cm mid-point of the upper 1 m). These are present day values (i.e., at global average temperature increase of ~1.1 °C). The equation was therefore constrained to ensure that (a) the value at a temperature anomaly of ~1.1 °C exceeded 2 °C, (b) the range at high levels of warming reached the weighted mean of 3.3 °C. An arbitrary upper limit of 3.5 °C was chosen.

The response of post-fire change in ground temperature (gT_Δ, Eq. (4)) to global average temperature increase was modeled as a sigmoidal response on the basis that at very high levels of warming, further increases in fire severity (and consequently post-fire ground heating) may become limited, for example by changes in fuel load (Supplementary Fig. 4.3[62]:

$$gT_\Delta = \frac{3.5}{1 + e^{-0.5 \times dT}} \quad (4)$$

While the majority of these data were collected within less than a decade of fire occurrence, they demonstrate that fire affects ground temperature over multiple years. However, due to the lack of studies that monitor post-fire ground temperature change over time and the likelihood of high spatial heterogeneity in the trajectory of post-fire ground temperature change (due to, for example, hydrological factors, burn severity and vegetation recovery), a conservative assumption was made here that fire could drive the development of additional abrupt thaw area for only one year following fire (Supplementary Table 5).

Emissions from fire-induced abrupt thaw. Emissions associated with fire-induced abrupt thaw were parameterized for each stage of abrupt thaw progression, as described in Method Section "Emissions from abrupt thaw". Emission parameters for fire-induced abrupt thaw were calculated as the difference between the 'undisturbed' annual net carbon balance and that of the specified stage of abrupt thaw (e.g., active thaw) as stated in Turetsky et al.[21]. This prevents 'double-counting' that could otherwise result from adding 'new' active abrupt thaw land in the fire-induced thaw module while also counting emissions from that same unchanged area of undisturbed land in the abrupt thaw module.

Fire-induced progressive thaw. Progressive gradual thaw of the upper 3 m of permafrost may be triggered when a severe fire removes a large proportion of the soil organic layer[63–65] or result from talik development followed by ongoing thaw from both above and below[29,30]. Recognizing the limited availability of empirical or modeled assessments of post-fire progressive thaw, we estimated an area affected by progressive thaw using a temperature response function applied to the remaining burned area (i.e., total burned area minus that affected by post-fire abrupt thaw) (Supplementary Fig. 5.1). According to this response, the proportion of remaining burned area that undergoes progressive thaw increases sigmoidally from 0 to a maximum of 0.25 (25%). The shape of this curve reflects the assumptions that under high levels of warming, fire return intervals will be shorter, and the active layer will be deeper, meaning that any given fire will be less likely to initiate progressive thaw for the first time (either because a previous burn has initiated progressive thaw, or because the permafrost table is otherwise absent or very deep). The maximum, approached only under high levels of global average temperature increase (>5 °C), was guided by the characterization of progressive thaw as a response only to severe fires, and on evidence indicating lower resilience to progressive thaw in uplands[66]. While there is no spatial distinction beyond the biome level in the context of fire-induced progressive thaw, around 25% of thermokarst-vulnerable landscapes are uplands[40], suggesting the maximum area available for progressive thaw should not be substantially higher than this figure. The thaw trajectory was modeled as a simple positive correlation between thaw depth and time since fire using data extracted from Jafarov et al.[66]; Supplementary Fig. 5.2). The volume of thawed permafrost was converted to a thawed carbon pool using average carbon densities for near surface (upper 3 m) permafrost of 21 kg m^{-2} and 19 kg m^{-2} for boreal and tundra biomes, respectively[67].

Fire-induced transient thaw. The remaining proportion of burned area unaffected by either abrupt or progressive thaw underwent transient thaw.

To determine thaw depth in the area affected by post-fire transient thaw, we used a function based on a well-established pattern of post-fire thaw and recovery: a gradual increase in thaw depth peaking within a decade of fire, followed by a gradual, slower period of recovery to pre-fire levels taking place over a decadal timescale, represented here using a Weibull curve[29,68,69] (Supplementary Fig. 5.3). While the simplified approach taken here distinguished only between the boreal and tundra biomes, the manifestation of this pattern in reality - including the extent of the increase in thaw depth and the duration (and likelihood) of recovery – also varies considerably with landscape and vegetation type[68]. The function was constrained by literature-derived empirical data Supplementary Table 1), that were corrected for the effects of ground subsidence, which can result in underestimated thaw depths[70]. To correct for subsidence, we used published data to calculate a ratio of ground subsidence to thaw depth change (average 0.39 cm cm^{-1}; Supplementary Table 2). Given the current state of knowledge and data availability, we derived a correction factor reflecting an average of studies conducted in different permafrost environments (Supplementary Table 2). However, given that emissions from post-fire permafrost thaw were small (Fig. 1) any over- or underestimation would have a relatively small impact on overall emissions. The volume of thawed permafrost was converted to a thawed carbon pool using the average carbon densities for near surface permafrost reported in Method Section "Fire-induced progressive thaw"[67].

Uncertainty. Uncertainty in the gradual thaw module reflects structural differences across the four land surface models[4], while the additional modules (abrupt thaw, combustion, and post-fire) include parameter uncertainty introduced through 500 ensemble configurations. A detailed description of uncertainty is provided in Supplementary Note 7.

Emission budgets

OSCAR set-up. Emissions budgets were estimated in the absence of permafrost or fire-related processes, and then with permafrost and fire-related processes 'switched on' in a stepwise manner (gradual thaw to post-fire thaw; Table 1). All budgets were calculated for four different SSP scenarios (SSP1–2.6; SSP2–4.5; SSP4–6.0; SSP5–8.5), and budgets which incorporated permafrost processes were estimated for each of the four LSMs used to drive the gradual thaw emulator. Results for SSP5–8.5 are only shown in the Supplementary Information because the main text focuses on mitigation-relevant pathways.

Our primary method to estimate emissions budgets for each simulation used an 'avoidance' approach, which defines the budget as the maximum cumulative CO_2 emissions below which the specified temperature threshold is avoided (i.e., not exceeded). This approach is consistent with methodology used in the IPCC 6th Assessment Report[35]. We also calculated emissions budgets using an 'exceedance' approach (S1.2), which was used for IPCC emissions budgets prior to the 6th Assessment Report. For exceedance budget estimates, budgets are defined as the cumulative CO_2 emissions reached at the point that global temperature equals a given threshold in a modeled scenario where global temperatures continue on to

Table 1 | Simulation sets show different configurations under which OSCAR was run

Simulation set	Gradual thaw Gasser et al.[4]	Abrupt thaw Section "Abrupt thaw module"	Combustion Section "Combustion emissions module"	Post-fire thaw Section "Post-fire permafrost thaw module"	LSM configurations
No Permafrost					1
A	X				4
B	X	X			4
C	X	X	X		4
D	X	X	X	X	4

Sections refer to Online Methods.
'Gradual thaw' includes 4 different configurations based on 4 LSMs; JSBACH, ORCHIDEE-MICT and two versions of JULES.

exceed that threshold (Supplementary Fig. 1.1). Each avoidance budget was run across a range of 'peak and decline' emissions pathways to ensure the specified temperature threshold was genuinely avoided (Supplementary Fig. 1.1).

Budget protocol. Emissions budgets were estimated based on 'additional warming', or the difference in temperature between a specified temperature threshold (i.e., 1.5 °C or 2 °C) and observed temperature change during 2012–2021 (T_{base}; Supplementary Note 1.3). This minimizes the impact of, for example, discrepancies between observed and modeled relationships between warming and cumulative emissions over time on the estimated emissions budgets[71–73]. For each simulation (i), where T^i is the simulated global mean temperature anomaly, we calculated maximum additional warming in °Celsius ($T^i_{\max}$, Eq. (5)):

$$T^i_{max} = maxT^i - T_{base} \quad (5)$$

We then calculated maximum cumulative CO_2 emissions ($B^i_{\max}$, Eq. (6)):

$$B^i_{max} = max\int_{t_{base}}^{t_f} E^i_{FF} + E^i_{LUC}dt \quad (6)$$

Where t_{base} refers to 2025 and t_f is the final year of the simulation (2150) and E_{ff} and E_{LUC} are emissions from fossil fuel combustion and land use change respectively. Budgets are reported in terms of cumulative CO_2 emissions, while temperature evolution in OSCAR is driven by all anthropogenic climate forcers. Any simulations in which either maximum additional cumulative CO_2 emissions or maximum additional warming occurred in the final timestep were discarded. Because the maximum temperature of a given simulation may not be exactly equal to the specified temperature threshold, the precise values for avoidance budgets were obtained by interpolating linearly within a T_{max} value interval of ±0.5 °C around the level of additional warming associated with the specified temperature target (T_{target}, Eq. (7)):

$$T^i_{max} = (T_{target} - T_{base}) \pm 0.5^{\circ}C \quad (7)$$

Data availability

The data generated and analyzed for this study consist of processed datasets used directly to generate the figures and tables presented in the manuscript and Supplementary Information. These data are publicly available via the GitHub repository https://github.com/whrc/OSCAR_abrupt_postfire. Full OSCAR model output files are not provided at this stage due to their volume and complexity.

Code availability

The source code of OSCAR is available at https://github.com/tgasser/OSCAR.git. The version of OSCAR modified and used for this study is available at https://github.com/whrc/OSCAR_abrupt_postfire. This includes the values of all parameters added to OSCAR as part of this study and the historic and scenario forcings used.

Received: 7 October 2024; Accepted: 5 January 2026;
Published online: 24 January 2026

References

1. Schuur, E. A. G. et al. Permafrost and climate change: carbon cycle feedbacks from the warming Arctic. *Annu. Rev. Environ. Resour.* **47**, 343–371 (2022).
2. Hugelius, G. et al. Estimated stocks of circumpolar permafrost carbon with quantified uncertainty ranges and identified data gaps. *Biogeosciences* **11**, 6573–6593 (2014).
3. Smith, S. L., O'Neill, H. B., Isaksen, K., Noetzli, J. & Romanovsky, V. E. The changing thermal state of permafrost. *Nat. Rev. Earth Environ.* **3**, 10–23 (2022).
4. Gasser, T. et al. Path-dependent reductions in CO_2 emission budgets caused by permafrost carbon release. *Nat. Geosci.* **11**, 830–835 (2018).
5. McGuire, A. D. et al. Dependence of the evolution of carbon dynamics in the northern permafrost region on the trajectory of climate change. *Proc. Natl. Acad. Sci.* **115**, 3882–3887 (2018).
6. Koven, C. D. et al. A simplified, data-constrained approach to estimate the permafrost carbon–climate feedback. *Philos. Trans. R. Soc. A* **373**, 20140423 (2015).
7. Burke, E. J., Jones, C. D. & Koven, C. D. Estimating the permafrost-carbon climate response in the CMIP5 climate models using a simplified approach. *J. Clim.* **26**, 4897–4909 (2013).
8. MacDougall, A. H., Avis, C. A. & Weaver, A. J. Significant contribution to climate warming from the permafrost carbon feedback. *Nat. Geosci.* **5**, 719–721 (2012).
9. Zhuang, Q. et al. CO_2 and CH_4 exchanges between land ecosystems and the atmosphere in northern high latitudes over the 21st century. *Geophys. Res. Lett.* **33**, L17403 (2006).
10. Natali, S. M. et al. Incorporating permafrost into climate mitigation and adaptation policy. *Environ. Res. Lett.* **17**, 091001 (2022).
11. Schädel, C. et al. Earth system models must include permafrost carbon processes. *Nat. Clim. Chang.* **14**, 114–116 (2024).
12. Treharne, R., Rogers, B. M., Gasser, T., MacDonald, E. & Natali, S. Identifying Barriers to Estimating Carbon Release From Interacting Feedbacks in a Warming Arctic. *Front. Clim.* **3**, 716464 (2022).
13. Langer, M. et al. The evolution of Arctic permafrost over the last 3 centuries from ensemble simulations with the CryoGridLite permafrost model. *Cryosphere* **18**, 363–385 (2024).
14. Meredith, M. P. et al. *IPCC, 2019: IPCC Special Report on the Ocean and Cryosphere in a Changing Climate* (IPCC, 2020).
15. Chadburn, S. E. et al. An observation-based constraint on permafrost loss as a function of global warming. *Nat. Clim. Change* **7**, 340–344 (2017).

16. Koven, C. D., Riley, W. J. & Stern, A. Analysis of permafrost thermal dynamics and response to climate change in the CMIP5 Earth system models. *J. Clim.* **26**, 1877–1900 (2013).
17. Slater, A. G. & Lawrence, D. M. Diagnosing present and future permafrost from climate models. *J. Clim.* **26**, 5608–5623 (2013).
18. Webb, H. et al. A review of abrupt permafrost thaw: definitions, usage, and a proposed conceptual framework. *Curr. Clim. Change Rep.* **11**, 7 (2025).
19. Rodenhizer, H. et al. Abrupt permafrost thaw accelerates carbon dioxide and methane release at a tussock tundra site. *Arct. Antarct. Alp. Res.* **54**, 443–464 (2022).
20. Costard, F. et al. Retrogressive thaw slumps on ice-rich permafrost under degradation: results from a large-scale laboratory simulation. *Geophys. Res. Lett.* **48**, e2020GL091070 (2021).
21. Turetsky, M. R. et al. Carbon release through abrupt permafrost thaw. *Nat. Geosci.* **13**, 138–143 (2020).
22. Zheng, B. et al. Record-high CO_2 emissions from boreal fires in 2021. *Science* **379**, 912–917 (2023).
23. Descals, A. et al. Unprecedented fire activity above the Arctic Circle linked to rising temperatures. *Science* **378**, 532–537 (2022).
24. Scholten, R. C., Coumou, D., Luo, F. & Veraverbeke, S. Early snowmelt and polar jet dynamics co-influence recent extreme Siberian fire seasons. *Science* **378**, 1005–1009 (2022).
25. McCarty, J. L. et al. Reviews and syntheses: Arctic fire regimes and emissions in the 21st century. *Biogeosciences* **18**, 5053–5083 (2021).
26. Byrne, B. et al. Carbon emissions from the 2023 Canadian wildfires. *Nature* **633**, 835–839 (2024).
27. Talucci, A. C. et al. Permafrost–wildfire interactions: active layer thickness estimates for paired burned and unburned sites in northern high latitudes. *Earth Syst. Sci. Data* **17**, 2887–2909 (2025).
28. Li, X.-Y. et al. Influences of forest fires on the permafrost environment: a review. *Adv. Clim. Change Res.* **12**, 48–65 (2021).
29. Holloway, J. E. et al. Impact of wildfire on permafrost landscapes: a review of recent advances and future prospects. *Permafr. Periglac. Process.* **31**, 371–382 (2020).
30. Gibson, C. M. et al. Wildfire as a major driver of recent permafrost thaw in boreal peatlands. *Nat. Commun.* **9**, 3041 (2018).
31. Chen, Y. et al. Future increases in Arctic lightning and fire risk for permafrost carbon. *Nat. Clim. Chang.* **11**, 404–410 (2021).
32. Veraverbeke, S. et al. Direct and longer-term carbon emissions from arctic-boreal fires: a short review of recent advances. *Curr. Opin. Environ. Sci. Health* **23**, 100277 (2021).
33. Walker, X. J. et al. Fuel availability not fire weather controls boreal wildfire severity and carbon emissions. *Nat. Clim. Chang.* **10**, 1130–1136 (2020).
34. Potter, S. et al. Burned area and carbon emissions across northwestern boreal North America from 2001–2019. *Biogeosciences* **20**, 2785–2804 (2023).
35. Canadell, J. G. et al. Global carbon and other biogeochemical cycles and feedbacks. In *Climate Change 2021: The Physical Science Basis. Contribution of Working Group I to the Sixth Assessment Report of the Intergovernmental Panel on Climate Change* (eds Masson-Delmotte, V. et al.) 673–816 (Cambridge University Press, 2021). https://doi.org/10.1017/9781009157896.001.
36. Gasser, T. et al. The compact Earth system model OSCAR v2.2: description and first results. *Geosci. Model Dev.* **10**, 271–319 (2017).
37. Natali, S. M. et al. Permafrost carbon feedbacks threaten global climate goals. *Proc. Natl. Acad. Sci.* **118**, e2100163118 (2021).
38. Friedlingstein, P. et al. Global carbon budget 2024. *Earth Syst. Sci. Data* **17**, 965–1039 (2025).
39. Schuur, E. A. G. et al. Vulnerability of permafrost carbon to climate change: implications for the global carbon cycle. *Bioscience* **58**, 701–714 (2008).
40. Olefeldt, D. et al. Circumpolar distribution and carbon storage of thermokarst landscapes. *Nat. Commun.* **7**, 13043 (2016).
41. Karjalainen, O., Aalto, J., Kanevskiy, M. Z., Luoto, M. & Hjort, J. High-resolution predictions of ground ice content for the Northern Hemisphere permafrost region. *Earth Syst. Sci. Data Discussions* 1–40, https://doi.org/10.5194/essd-2022-144 (2022).
42. Zwieback, S. & Meyer, F. J. Top-of-permafrost ground ice indicated by remotely sensed late-season subsidence. *Cryosphere* **15**, 2041–2055 (2021).
43. Kokelj, S. V., Lantz, T. C., Tunnicliffe, J., Segal, R. & Lacelle, D. Climate-driven thaw of permafrost preserved glacial landscapes, northwestern Canada. *Geology* https://doi.org/10.1130/g38626.1 (2017).
44. Langer, M. et al. Rapid degradation of permafrost underneath waterbodies in tundra landscapes-Toward a representation of thermokarst in land surface models. *J. Geophys. Res.Earth Surf.* **121**, 2446–2470 (2016).
45. Plaza, C. et al. Direct observation of permafrost degradation and rapid soil carbon loss in tundra. *Nat. Geosci.* **12**, 627–631 (2019).
46. de Vrese, P. & Brovkin, V. Timescales of the permafrost carbon cycle and legacy effects of temperature overshoot scenarios. *Nat. Commun.* **12**, 2688 (2021).
47. Gasser, T. et al. Historical CO_2 emissions from land use and land cover change and their uncertainty. *Biogeosciences* **17**, 4075–4101 (2020).
48. Guimberteau, M. et al. ORCHIDEE-MICT (v8.4.1), a land surface model for the high latitudes: model description and validation. *Geosci. Model Dev.* **11**, 121–163 (2018).
49. Burke, E. J., Chadburn, S. E. & Ekici, A. A vertical representation of soil carbon in the JULES land surface scheme (vn4.3-permafrost) with a focus on permafrost regions. *Geosci. Model Dev.* **10**, 959–975 (2017).
50. Burke, E. J. et al. Quantifying uncertainties of permafrost carbon–climate feedbacks. *Biogeosciences* **14**, 3051–3066 (2017).
51. Giorgetta, M. A. et al. Climate and carbon cycle changes from 1850 to 2100 in MPI-ESM simulations for the Coupled Model Intercomparison Project phase 5. *J. Adv. Model. Earth Syst.* **5**, 572–597 (2013).
52. Meinshausen, M. et al. The shared socio-economic pathway (SSP) greenhouse gas concentrations and their extensions to 2500. *Geosci. Model Dev.* **13**, 3571–3605 (2020).
53. Hurtt, G. C. et al. Harmonization of global land use change and management for the period 850–2100 (LUH2) for CMIP6. *Geosci. Model Dev.* **13**, 5425–5464 (2020).
54. Moubarak, M., Sistla, S., Potter, S., Natali, S. M. & Rogers, B. M. Carbon emissions and radiative forcings from tundra wildfires in the Yukon–Kuskokwim River Delta, Alaska. *Biogeosciences* **20**, 1537–1557 (2023).
55. Smith, M. A., Cain, M. & Allen, M. R. Further improvement of warming-equivalent emissions calculation. *npj Clim. Atmos. Sci.* **4**, 19 (2021).
56. Posit team. RStudio: Integrated Development Environment for R. Posit Software, PBC, Boston, MA. (2023). http://www.posit.co/.
57. Dinerstein, E. et al. An ecoregion-based approach to protecting half the terrestrial realm. *BioScience* **67**, 534–545 (2017).
58. Veraverbeke, S., Rogers, B. M. & Randerson, J. T. Daily burned area and carbon emissions from boreal fires in Alaska. *Biogeosciences* **12**, 3579–3601 (2015).
59. Phillips, C. A. et al. Escalating carbon emissions from North American boreal forest wildfires and the climate mitigation potential of fire management. *Sci. Adv.* **8**, eabl7161 (2022).
60. Akagi, S. K. et al. Emission factors for open and domestic biomass burning for use in atmospheric models. *Atmos. Chem. Phys.* **11**, 4039–4072 (2011).
61. van der Werf, G. R. et al. Global fire emissions estimates during 1997–2016. *Earth Syst. Sci. Data* **9**, 697–720 (2017).
62. Foster, A. C. et al. Bottom-up drivers of future fire regimes in western boreal North America. *Environ. Res. Lett.* **17**, 025006 (2022).
63. Fisher, J. P. et al. The influence of vegetation and soil characteristics on active-layer thickness of permafrost soils in boreal forest. *Glob. Change Biol.* **22**, 3127–3140 (2016).

64. Loranty, M. M. et al. Siberian tundra ecosystem vegetation and carbon stocks four decades after wildfire. *J. Geophys. Res.* **119**, 2144–2154 (2014).
65. Nossov, D. R., Jorgenson, M. T., Kielland, K. & Kanevskiy, M. Z. Edaphic and microclimatic controls over permafrost response to fire in interior Alaska. *Environ. Res. Lett.* **8**, 035013 (2013).
66. Jafarov, E. E., Romanovsky, V. E., Genet, H., McGuire, A. D. & Marchenko, S. S. The effects of fire on the thermal stability of permafrost in lowland and upland black spruce forests of interior Alaska in a changing climate. *Environ. Res. Lett.* **8**, 35030–35030 (2013).
67. Hugelius, G. et al. The Northern Circumpolar Soil Carbon Database: spatially distributed datasets of soil coverage and soil carbon storage in the northern permafrost regions. *Earth Syst. Sci. Data* **5**, 3–13 (2013).
68. Zhang, Y., Wolfe, S. A., Morse, P. D., Olthof, I. & Fraser, R. H. Spatiotemporal impacts of wildfire and climate warming on permafrost across a subarctic region, Canada. *J. Geophys. Res. Earth Surf.* **120**, 2338–2356 (2015).
69. Rocha, A. V. et al. The footprint of Alaskan tundra fires during the past half-century: implications for surface properties and radiative forcing. *Environ. Res. Lett.* **7**, 44039–44039 (2012).
70. Rodenhizer, H. et al. Carbon thaw rate doubles when accounting for subsidence in a permafrost warming experiment. *J. Geophys. Res.* **125**, e2019JG005528 (2020).
71. Schurer, A. P. et al. Interpretations of the Paris climate target. *Nat. Geosci.* **11**, 220–221 (2018).
72. Millar, R. J. et al. Emission budgets and pathways consistent with limiting warming to 1.5 °C. *Nat. Geosci.* **10**, 741–747 (2017).
73. Leach, N. J. et al. Current level and rate of warming determine emissions budgets under ambitious mitigation. *Nat. Geosci.* **11**, 574–579 (2018).

Acknowledgements

Woodwell Climate Research Center is located on the traditional and sacred land of the Wampanoag people who still occupy this land, and whose history, language, traditional ways of life, and culture continue to influence this vibrant community. Our research occurs across the circumpolar Arctic, where Indigenous Peoples, such as the Yup'ik, Athabaskan cultures, Iñupiat, Alutiiq, Gwich'in, Inuit, Inuvialuit, Saami, Nenets, Khanty, Mansi, Evenk, Chukchi, and Kalaallit, have lived since time immemorial. R.T., B.R., S.N., T.S., and E.M. were supported by One Earth Foundation, Gordon and Betty Moore Foundation (#8414), Quadrature Climate Fund (QCF Prime Grant Number 01-21-000094), and with funding catalyzed through the Audacious Project (Permafrost Pathways). C.S. was supported with funding catalyzed through the Audacious Project (Permafrost Pathways). T.G. was supported by the European Union's Horizon 2020 and Horizon Europe research and innovation programs under grant agreements #773421 (Nunataryuk) and #101056939 (RESCUE). E Jafarov and S Potter provided guidance and support regarding fire-induced thaw processes and C Phillips provided guidance and support regarding below-ground combustion.

Author contributions

Schädel conducted the uncertainty analysis and final model runs, led the synthesis of results, substantially revised the manuscript, and updated the figures and tables. Treharne led the initial development of the abrupt thaw and wildfire model components, with extensive input from Gasser, and wrote the first draft of the manuscript. Gasser contributed to model development, implementation, and methodological guidance, and interpretation of results. MacDonald contributed to data extraction and compilation of model parameters. Natali and Rogers contributed to the conceptual development of the study, interpretation of results, and framing of the analysis. Turetsky provided conceptual input and methodological guidance on abrupt permafrost and wildfire disturbance processes. Smith was responsible for cloud computing infrastructure and computational support. All authors contributed to editing and revising the manuscript and approved the final version.

Competing interests

The authors declare no competing interests.

Additional information

Supplementary information The online version contains supplementary material available at https://doi.org/10.1038/s43247-026-03189-5.

Correspondence and requests for materials should be addressed to Christina Schädel.

Peer review information *Communications Earth and Environment* thanks the anonymous reviewers for their contribution to the peer review of this work. Primary Handling Editor: Alice Drinkwater. [A peer review file is available].